Pressure-controlled cavity expansion in clay

Alfred S.K. Au, Albert T. Yeung, and Kenichi Soga

Abstract: Experimental studies and numerical simulation of experiments were conducted on pressure-controlled cavity expansion in clay. The modified Cam-clay model was used to describe the clay behaviour. The experimental data are in good agreement with the simulation results, indicating that the adopted numerical simulation procedure is a plausible and reliable technique to study the fundamental behaviour of pressure-controlled cavity expansion. A new parameter, cavity aspect ratio (CAR), was defined to better describe the cavity shape. Different phenomena during the cavity expansion process are thus studied numerically, and the results are presented in this paper.

Key words: pressure-controlled cavity expansion, numerical simulation, laboratory investigation, modified Cam-clay model, cavity aspect ratio (CAR), ABAQUS.

Résumé : On a réalisé des études expérimentales et une simulation numérique d'expériences sur l'expansion d'une cavité dans l'argile. Le modèle Cam-clay modifié a été utilisé pour décrire le comportement de l'argile. Les données expérimentales concordent bien avec les résultats de la simulation, ce qui indique que la procédure de simulation numérique est une technique plausible et fiable pour étudier le comportement fondamental de l'expansion d'une cavité sous pression contrôlée. On a défini un nouveau paramètre, le rapport d'aspect de la cavité (CAR), pour mieux décrire la forme de la cavité. Différents phénomènes durant le processus d'expansion de la cavité ont alors été étudiés numériquement, et les résultats sont présentés dans cet article.

Mots clés : expansion de cavité sous pression contrôlée, simulation numérique, étude en laboratoire, modèle Cam-clay modifié, rapport d'aspect de la cavité (CAR), ABAQUS.

[Traduit par la Rédaction]

Introduction

Many analytical solutions are available for cylindrical and spherical cavity expansion problems in elastoplastic materials (Hill 1950; Vesić 1972; Carter et al. 1986; Yu and Houlsby 1991; Collins and Stimpson 1994; Collins and Yu 1996; Bolton and Whittle 1999; Yu and Rowe 1999; Kovacevic et al. 2000; Cao et al. 2001; Chang et al. 2001; Salgado and Randolph 2001; El-Kelesh et al. 2001; Hsieh et al. 2002; Schnaid and Mantaras 2003). These applications in geomechanics are being developed to model the behaviour of geomaterials during pressuremeter testing, cone penetration testing, pile driving, compaction grouting, cratering by explosives, tunneling, etc. and to determine the ultimate bearing capacity of piles, the breakout resistance of anchors, etc. The degree of success of these applications of the cavity expansion theory in solving these geomechanical problems varies, however. Therefore, the limitations of the theory should be noted.

On the basis of the boundary condition of the cavity, solutions to problems of cavity expansion can be broadly classified into two categories: (*i*) pressure-controlled cavity expansion, and (*ii*) displacement-controlled cavity expansion. Spatial distribution of pressure expanding the cavity is uniform throughout the pressure-controlled cavity expansion process and is a function of time only, regardless of the deforming shape of the cavity. On the contrary, the cavity remains spherical or cylindrical throughout the displacement-controlled cavity expansion process. Most analytical solutions are derived for spherical or cylindrical displacement-controlled cavity expansion in an infinite, homogeneous, and isotropic continuum under an isotropic stress state. The soil behaves as an elastic medium until the onset of yield defined by the Mohr–Coulomb or Cam-clay criterion. The displacements in the medium are thus radial everywhere, and the analysis is therefore essentially one-dimensional. Most available solutions are for cavity expansion under either undrained conditions, i.e., no volume change, or drained conditions, i.e., no excess pore-water pressure.

These assumptions are practically valid for the description of penetration of cone penetrometers, driven piles, etc. Therefore, analytical solutions to displacement-controlled undrained cavity expansion problems may be adequate to provide solutions to such geotechnical engineering problems. However, compaction grouting, pressuremeter tests, cratering by explosives, breakout resistance of anchors, etc. are better categorized as pressure-controlled cavity expansion problems. For example, depending on the initial stress and boundary conditions, the grout bulb created by compaction grouting may be nonspherical. Therefore, it is evident that existing analytical solutions may not be adequate in solving these geotechnical engineering problems. This inves-

Received 1 February 2005. Accepted 21 February 2006. Published on the NRC Research Press Web site at http://cgj.nrc.ca on 29 June 2006.

A.S.K. Au and A.T. Yeung.[1] Department of Civil Engineering, The University of Hong Kong, Pokfulam Road, Hong Kong, China.
K. Soga. Department of Engineering, University of Cambridge, Cambridge CB2 1PZ, UK.

[1]Corresponding author (e-mail: yeungat@hkucc.hku.hk).

Fig. 1. Schematic of the experimental setup of grout injection. CPU, central processing unit; LVDT, linear variable displacement transducer; PIC, pressure interface chamber.

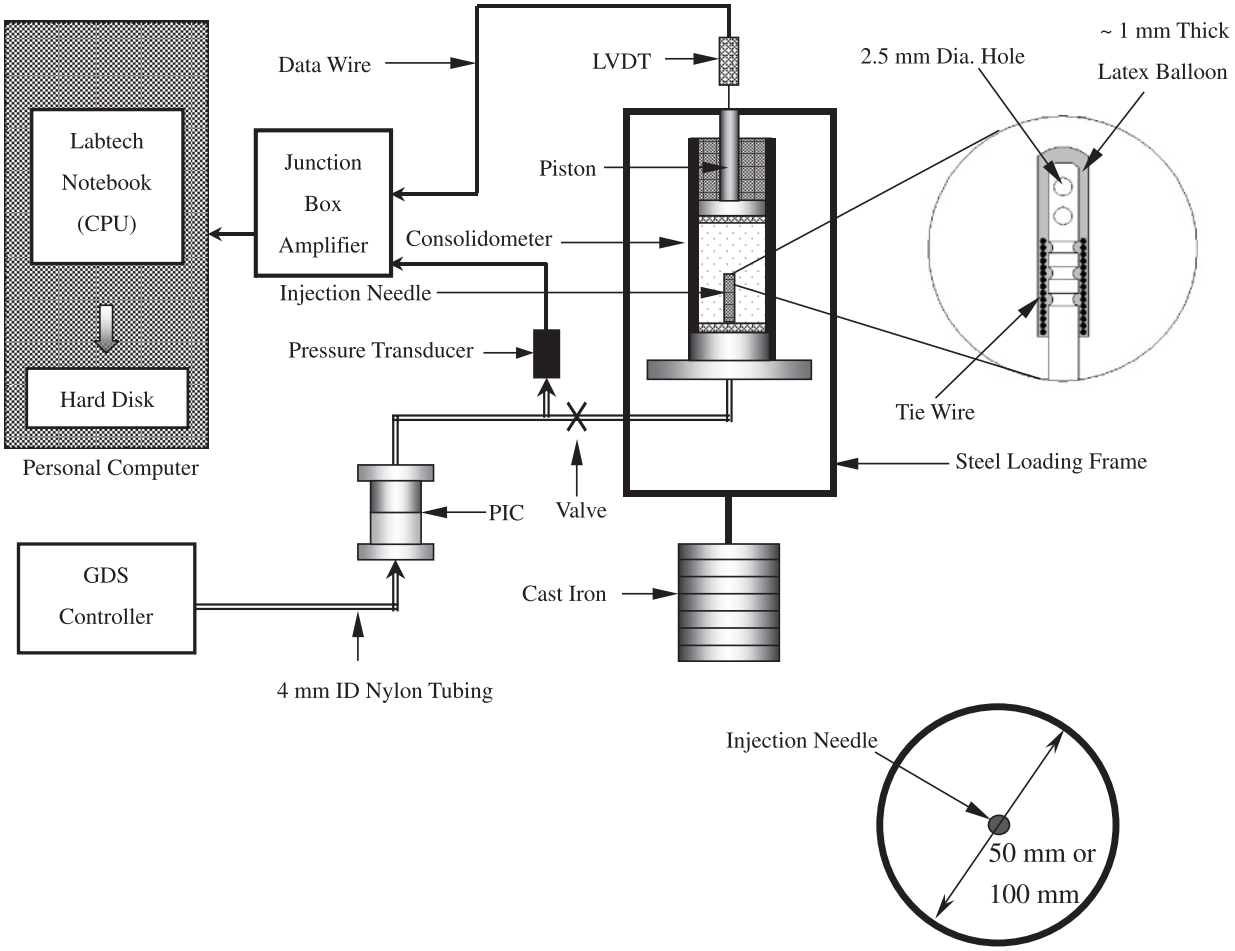

tigation was conducted to develop a better understanding of the pressure-controlled cavity expansion process in clay with intended applications in compaction grouting. Laboratory-scale grouting experiments were performed and numerical simulations of soil behaviour during the grouting process were conducted using finite element analyses. Soil deformations around the expanding cavity were examined. The experimental data were compared with the results of numerical simulations to establish the validity of numerical analyses. Details of the investigation are reported in this paper.

Laboratory experimental investigation

Pressure-controlled cavities were expanded in clay specimens by precisely controlled injection of epoxy resin or water into a tailor-made latex balloon through a multiple-hole injection needle embedded in the clay specimen. Clay specimens of different initial conditions, such as specimen diameter, preconsolidation pressure, and overconsolidation ratio (OCR), were prepared in specifically modified consolidometers. Epoxy resin was used to capture the final shape of the cavity. The laboratory-scale experimental apparatus specifically designed, fabricated, and assembled is shown in Fig. 1. Only a brief description of the apparatus and experimental procedure are given here, and readers interested in the details of the apparatus should refer to Au (2001), Soga et al. (2004), and Au et al. (2006).

Clay specimens were consolidated in modified consolidometers with internal diameters of 50 mm (denoted as R25 specimens) and 100 mm (denoted as R50 specimens) and height of 280 mm, accommodating specimens 100 mm in height. The consolidation stress or vertical effective stress was exerted on the specimen by cast iron weights through a loading frame and a piston as shown in Fig. 1. A hole was drilled at the centre of the base of the modified consolidometer to install an injection needle. Copper needles of 4 mm outer diameter and 3 mm internal diameter with the tip installed at 50 mm above the specimen base were used as injection needles. Two 2.4 mm diameter holes were drilled through the injection needle near the tip to allow injection of fluid through the needle in a horizontal direction to inflate the latex balloon as shown in Fig. 1. Three 0.2 mm wide grooves were machined approximately 15 mm below the tip of the needle as shown. The tip of the injection needle was trimmed to allow even spread of latex around the tip. A latex membrane approximately 1 mm thick was installed at the tip of the injection needle to be inflated to simulate cavity expansion. After the latex membrane cured, the outside surface was greased to minimize any potential shearing damage induced by interactions between clay and latex membrane dur-

Fig. 2. Heave versus time during grout injection.

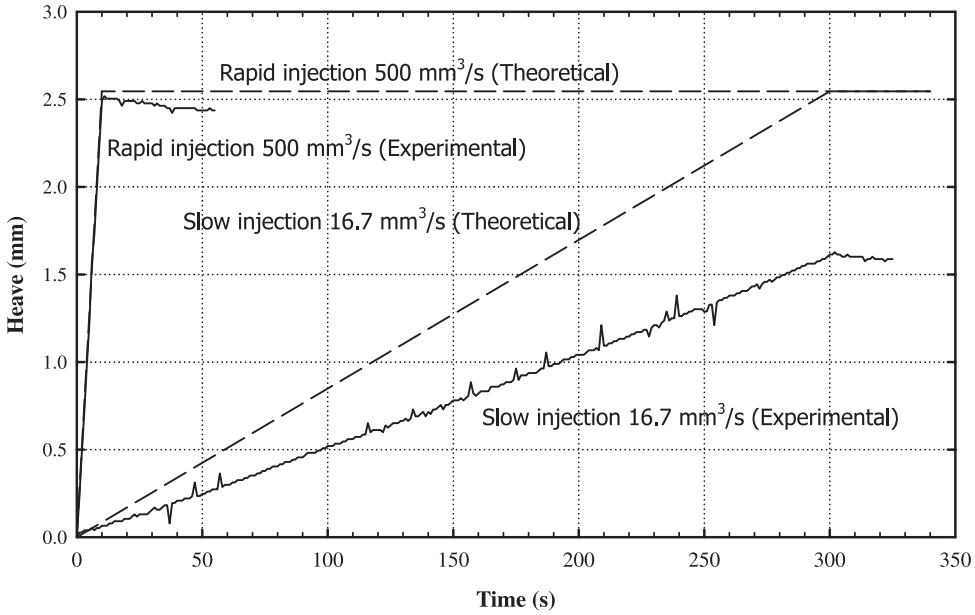

ing injection. The valve installed at the entry point of each needle was then closed to ensure no gas bubble was trapped in the injection system.

The fluid was injected using a GDS pressure–volume controller (GDS Instruments, Hook, UK), which can control the rate of injection volume and limit the maximum injection pressure. A pressure interface chamber (PIC) was used, when necessary, to transmit the pressure from the deaired water in the GDS controller to the injection fluid. During injection, the injection volume, vertical displacement of the top surface of the clay specimen, and injection pressure were measured by GDS, linear variable displacement transducer (LVDT), and pressure transducer as shown in Fig. 1, respectively. Post-injection settlement was continuously measured as a function of time to assess the progress of consolidation following the cavity expansion process. Methodologies to correct for pressure losses due to friction of fluid flow within the system and expansion of the latex membrane have been developed and presented by Au et al. (2006). Frictional loss between the specimen and the vertical cylindrical surface of the modified consolidometer measured by Au (2001) is negligible. Therefore, volume change of the expanding cavity and the resulting pressure exerted on the clay can be accurately determined.

E-grade kaolin was used for the experiment. The Cam-clay parameters of the material obtained by triaxial tests are as follows: $\kappa = 0.03$, $\lambda = 0.13$, $M = 1.05$, $\Gamma = 2.65$, $\upsilon = 0.2$, and $k = 2 \times 10^{-9}$ m/s, where κ is the slope of the unloading–reloading line in the $v - \ln p'$ plane; v is the specific volume; p' is the mean effective stress; λ is the slope of the normal compression line in the $v - \ln p'$ plane; M is the slope of the critical state line; Γ is the location of the critical state line in the compression plane; υ is the Poisson's ratio of the material; and k is the hydraulic conductivity of the material. A detailed description of the material is given by Elmes (1985).

The vertical effective stress exerted on the specimen was maintained at 140 kPa, simulating a typical depth of overburden during compaction grouting, i.e., at a depth of approximately 10–15 m below the ground surface. Clay specimens were prepared at OCRs of 1.0, 1.5, 2.0, and 5.0 to investigate the influence of stress histories on the cavity expansion process. Vertical displacement of the top surface of the specimen was measured as a function of time throughout the test to quantify the vertical soil displacement induced by expansion of the cavity and subsequent consolidation. Theoretically, the surface should heave 2.55 and 0.61 mm, respectively, for the R25 and R50 specimens under undrained conditions, i.e., no volume change of clay, for an injection volume of 5000 mm^3. Measured surface heaves as a function of time during injection at two different rates, i.e., 500 mm^3/s (rapid) and 16.7 mm^3/s (slow), for the R25 specimens are shown in Fig. 2. It can be observed that both surface heaves increase linearly with time during injection, but the maximum heaves induced at the rapid and slow injection rates are 2.53 and 1.72 mm, respectively, indicating the degree of consolidation that occurred during injection is negligible when the injection rate is rapid but significant when the injection rate is slow. The deviation between injected volume and heave volume as a function of time during injection further substantiates the observation.

Development of numerical model

A numerical model was developed to simulate the laboratory experiment and establish the validity of the modeling process. It includes the clay specimen and the base of the loading piston and is a two-dimensional axisymmetric model for computational efficiency. The dimensions of the components used in the numerical model are identical to those in the experiments. Therefore, the heights of the piston base and the clay specimen are 10 and 100 mm, respectively. Eight-node quadrilateral full integration consolidation elements and eight-node quadrilateral full integration elements (without consolidation) are adopted for the clay specimen and piston base, respectively. There are 1571 elements in the mesh of the R50 specimen and 1336 elements in the mesh of

Fig. 3. Numerical model: (*a*) R50 specimen; (*b*) R25 specimen.

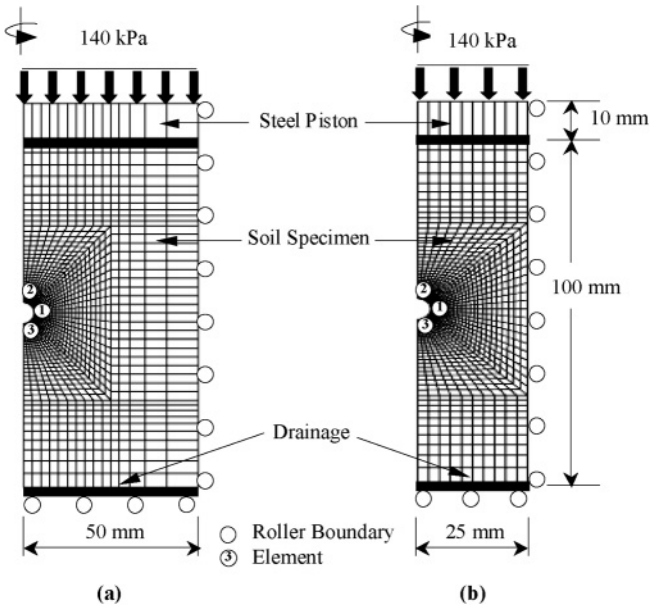

the R25 specimen, as shown in Fig. 3. Only elements whose stresses are reported and discussed later in the paper are numbered in Fig. 3. The size of the element increases with an increase in the radial distance from the cavity centre, where most rapid variations of various parameters with distance are expected to take place. Mesh adjustments have been conducted to ensure the number of elements in the numerical model is adequate to give an acceptable degree of accuracy. The vertical cylindrical boundary and the bottom boundary were modeled as roller boundaries. The modified Cam-clay model was used to describe the soil behaviour because the model can capture the plastic deformation behaviour of remolded clay reasonably well, which is the dominant mechanism in the vicinity of the injection point. The modified Cam-clay model implemented in ABAQUS (ABAQUS, Inc., Providence, R.I.), i.e., an extended version of the modified Cam-clay, was used in the analyses.

Simulation of initial geostatic conditions

Since the self-weight of the clay specimen is considerably smaller than the vertical stress exerted on the specimen, it was neglected in the analyses. The initial outside radius of the latex balloon was taken to be an internal fixed boundary. The laboratory specimens were consolidated to 140, 210, 280, and 700 kPa and then rebounded to 140 kPa to prepare specimens with OCRs of 1.0, 1.5, 2.0, and 5.0, respectively. In the numerical analysis, the initial stress was set at 140 kPa. The initial void ratio was set at the void ratio at 140 kPa for the normally consolidated specimen. For OCRs of 1.5, 2.0, and 5.0, void ratios at 140 kPa after rebound from the corresponding consolidation stresses were used as initial void ratios, and the corresponding preconsolidation pressures were used to simulate the required OCRs. The coefficient of lateral pressure at rest, K_0, was estimated by the following empirical relationship proposed by Schmidt (1966):

$$[1] \qquad K_0 = [1 - \sin(1.2\phi'_{crit})]\mathrm{OCR}^{\sin(1.2\phi'_{crit})}$$

Table 1. Summary of numerical simulations.

Simulation No.	OCR	Specimen radius (mm)
1	1.0	25
2	1.0	50
3	1.5	25
4	1.5	50
5	2.0	25
6	2.0	50
7	5.0	25
8	5.0	50

where ϕ'_{crit} is the critical state angle of shearing resistane. Using eq. [1], the estimated values of K_0 for OCRs of 1.0, 1.5, and 2.0 are less than unity while that for an OCR of 5.0 is greater than unity. The initial outside radius of the latex balloon was used as the initial radius of the cavity.

The nodal reaction forces around the cavity at equilibrium under geostatic conditions were first calculated. The same forces were then applied at the nodes of the cavity to maintain the initial spherical shape of the cavity. The inside boundary around the cavity was then removed before application of the grouting pressure.

Simulation of pressure-controlled cavity expansion

Simulations were conducted of the rapid pressure-controlled cavity expansion process under practically undrained conditions. After the geostatic state had been initialized, cavity expansion was simulated by rapidly increasing the pressure within the initial spherical cavity in equal steps. When the rate of pressure increase is greater than a threshold value to attain an overall undrained condition in the specimen, the simulation results are practically independent of the rate of pressure increase. The volume of the cavity was calculated after each pressure step to ensure the total experimental injection volume was not exceeded. The clay around the expanding cavity was expected to undergo large deformation. Therefore, geometric nonlinearity and updated Lagrangian formulation were adopted in the analyses. During the analyses, stresses and pore-water pressures in the clay were monitored for the development of plastic zone using one of the two criteria: (1) the stress state is at the interaction of the yield surface and the critical state line when the stress of any clay element attains the critical state; or (2) when any of the effective principal stresses in a clay element diminishes.

The simulation was terminated when the cavity was expanded to the target volume, i.e., 5000 mm^3, the total injection volume in the experiment.

Results and discussion

The simulations of eight pressure-controlled cavity expansion experiments as tabulated in Table 1 are presented. The results of numerical simulations are compared with the experimental data to establish the viability of the numerical simulation procedure. Variation of stresses and development of a failure–plastic zone in the vicinity of the cavity during the expansion process are evaluated to investigate various ef-

fects on the fundamental behaviour of pressure-controlled cavity expansion.

Evaluation of numerical simulation procedure

Cavity shape

The effects of stress history and radial boundary on cavity shape were evaluated experimentally and numerically. In cavity expansion experiments, 5000 mm^3 of epoxy resin was injected into the latex balloon so that the final cavity shape could be captured by the solidified epoxy resin. Some of these captured final cavity shapes are shown in Fig. 4. It can be observed that elliptical cavities with a major axis in the horizontal direction were formed in R25 specimens with OCRs of 1.0 and 1.5 as shown in Fig. 4*a*. Elliptical cavities with minor axes in the horizontal direction were formed in R50 specimens of similar stress history, however, as shown in Fig. 4*b*.

The deforming shapes of the cavity during the expansion process obtained by numerical simulations are presented in Fig. 5, where δV is the increase in cavity volume in mm^3. The shape of the cavity is presented in the *R*–*Z* plane, where *R* and *Z* are the horizontal and vertical distances from the centre of the cavity, respectively. It is evident from these simulations that the shape of the cavity depends on the OCR and distance from the boundary as observed in laboratory experiments.

A cavity aspect ratio (CAR) as shown in Fig. 6 is defined to better characterize the cavity shape. It is basically the ratio of the maximum horizontal dimension to the maximum vertical dimension of the cavity. Results of numerically simulated CAR during cavity expansion for R25 and R50 specimens with different OCRs are presented in Fig. 7.

For cavity expansion in soil specimens with K_0 less than unity, i.e., OCR ≤ 2, CAR decreases initially and then increases, regardless of the size of the specimen. For heavily overconsolidated clay, i.e., OCR = 5 and $K_0 > 1$, CAR increases monotonically with an increase in injection volume. For R25 specimens, values of CAR are generally greater than unity, indicating formation of cavities of elliptical shape with a major axis in the horizontal direction, as observed in the experiments. For R50 specimens, values of CAR are generally smaller than unity, with the exception of heavily overconsolidated specimens, indicating the formation of cavities of elliptical shape with a major axis in the vertical direction, as observed in the experiments. Moreover, it can be observed that CAR values of cavities in R25 specimens are always larger than those in R50 specimens at the same injection volume.

A comparison of the experimentally measured and numerically simulated values of CAR at an injection volume of 5000 mm^3 for different sizes of specimens with different OCRs is presented in Fig. 8. The broken line indicates prefect agreement between experimental data and numerical simulations. It can be observed that the experimental data are in good agreement with numerical simulations; however, experimentally measured CAR values in R25 specimens are always larger than those from the numerical simulations. The results reveal that CAR increases with an increase in OCR of the clay and a decrease in specimen diameter. These phenomena can be delineated by the results of numerical simulations revealing variation of stresses and development of a failure–plastic zone in the vicinity of the cavity during the expansion process.

Fig. 4. Shape of cavity under different conditions: (*a*) R25 specimens; (*b*) R50 specimens.

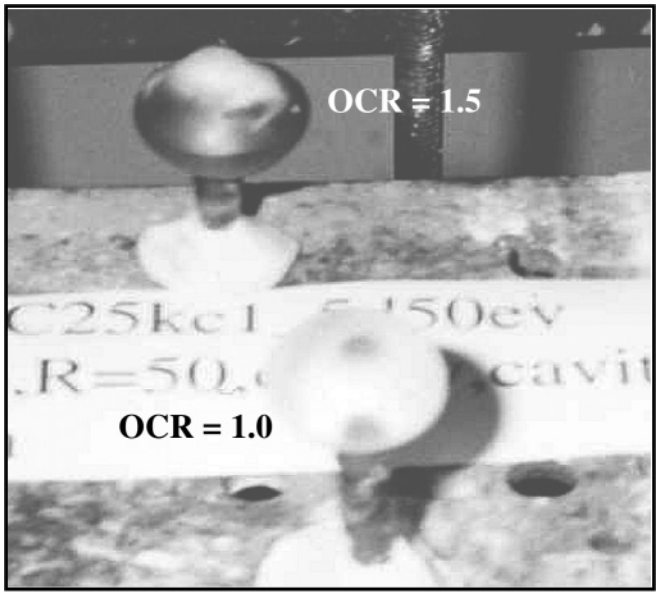

(a)

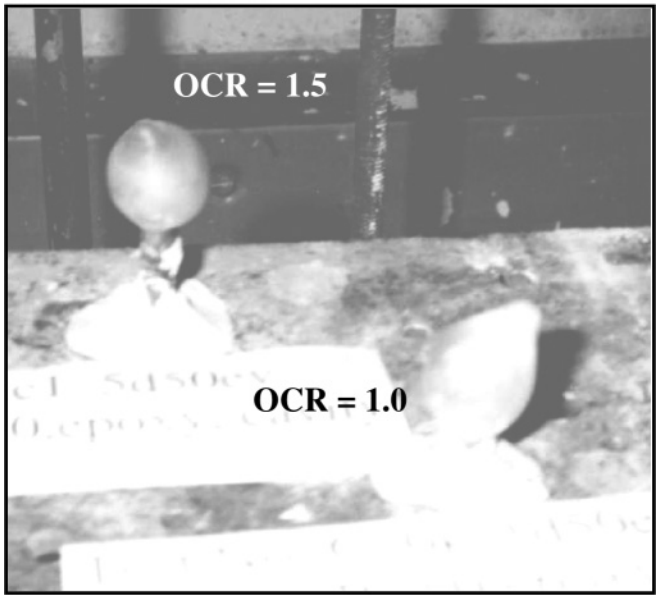

(b)

Injection pressure characteristics

A plot of experimentally measured injection pressure versus cavity volume for R50 specimens with different OCRs is presented in Fig. 9. As the cavity is being expanded, the injection pressure rises rapidly to a peak value. When the peak injection pressure has been reached, further expansion of the cavity does not require any increase in injection pressure, indicating the formation of a plastic zone around the cavity.

Fig. 5. Numerically simulated cavity shape during cavity expansion: (*a*) R50 specimen with OCR = 2.0; (*b*) R25 specimen with OCR = 1.0.

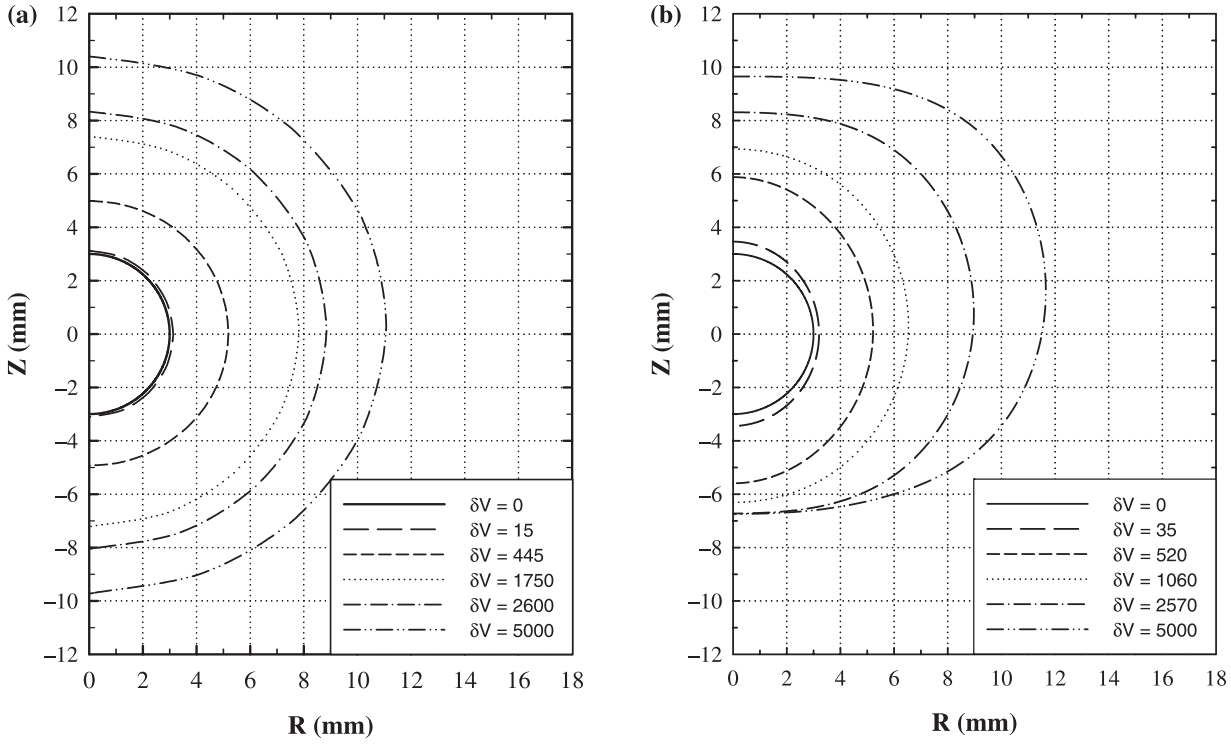

Fig. 6. Definition of cavity aspect ratio (CAR).

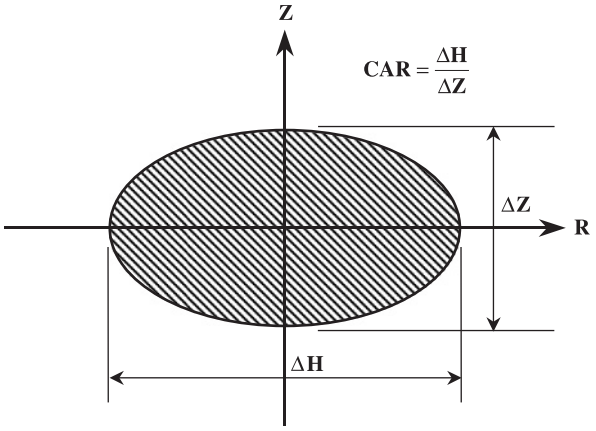

The experimental results also demonstrate that the peak injection pressure increases with an increase in the OCR of the clay, as the undrained shear strength of the clay increases with an increase in its OCR.

A comparison of the numerically simulated and experimentally measured peak injection pressure for specimens of different sizes and OCRs is presented in Fig. 10. The broken line indicates prefect agreement between experimental data and numerical simulations. It can be observed that the effect of specimen size on the peak injection pressure is very small, indicating the peak injection pressure is dictated by the plastic zone in the clay in the immediate vicinity of the cavity. Although the numerically simulated peak injection pressure is consistently higher than the respective experimental value, the numerical simulations are in good agreement with the experimental data except for heavily overconsolidated clay. Two factors that have not been taken into account in the numerical simulation may have contributed to the discrepancy between the numerical simulations and experimental data for the specimen with OCR of 5.0: (*i*) yielding of heavily overconsolidated clay may be better described by the Hvorslev yield surface rather than by the dry side of the modified Cam-clay yield surface (a detailed description of the two different yield surfaces is given by Atkinson and Bransby 1978); and (*ii*) the brittleness of heavily overconsolidated clay may lead to formation of microcracks around the expanding cavity, resulting in significant reduction of undrained shear strength of the clay.

Soil behaviour during pressure-controlled cavity expansion

Distribution of excess pore-water pressure

The average of excess pore-water pressures in the immediate vicinity of the cavity in a normally consolidated R50 specimen as a function of injection volume is presented in Fig. 11. The average excess pore-water pressure is obtained by averaging the excess pore-water pressure of the clay elements on the expanding surface of the cavity. The injection pressure is also shown for comparison. It can be observed in Fig. 11 that the average excess pore-water pressure in the immediate vicinity of the cavity is considerably lower than the injection pressure, indicating that localized redistribution of excess pore-water pressure in the clay around the cavity is considerable, although the overall volume change of the clay is negligible, as shown in Fig. 2. Similar analytical results are presented by Collins and Yu (1996).

Fig. 7. Numerically simulated CAR during cavity expansion: (*a*) R25 specimen; (*b*) R50 specimen.

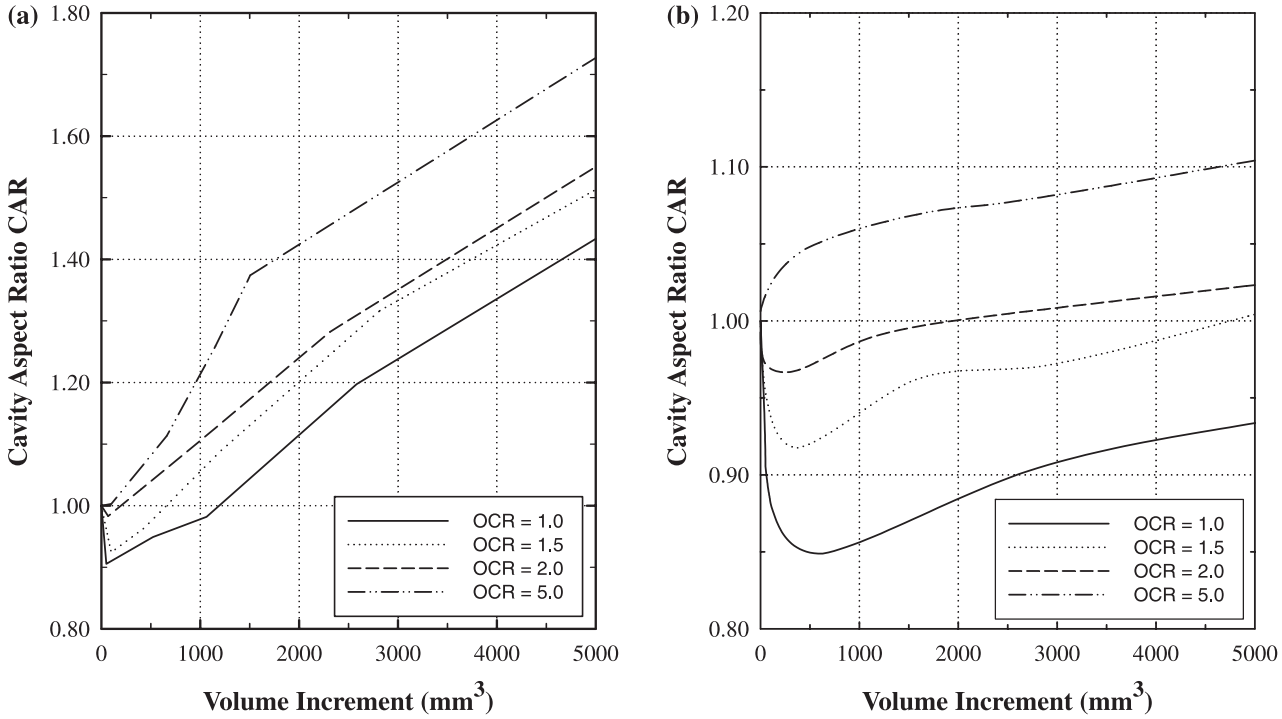

Fig. 8. Comparison of numerically simulated and experimentally measured CAR.

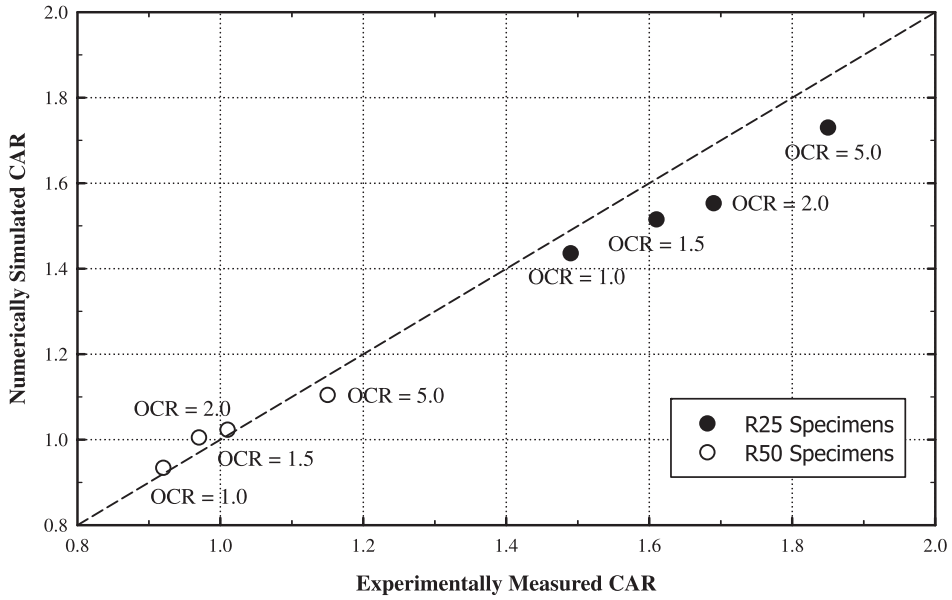

Distributions of excess pore-water pressure along the *R* axis at different injection volumes are presented in Fig. 12. The increase in excess pore-water pressure induced by cavity expansion decreases rapidly with distance from the cavity centre. The effects of the vertical cylindrical boundary become apparent when the injection volume increases, however.

Distribution of principal stresses and propagation of cavity

The *R* and *Z* directions are depicted in Fig. 6, and the circumferential direction *T* is defined as the direction of the normal to the *R*–*Z* plane. Results of numerical simulations indicate that shear stresses in the elements on the *R* and *Z* axes are negligibly small, indicating that the principal axes of these elements are approximately in the *R*, *Z*, and *T* directions. These results are quite trivial from the approximate symmetry of the problem. Strictly speaking, the *R* and *T* axes are not axes of symmetry, as the top and bottom boundaries are not identical. Variations of stresses are monitored during the expansion process in elements 1–3 in the specimen as shown in Fig. 3. Element 1 is on the *R* axis at a dis-

Fig. 9. Experimentally measured injection pressure versus cavity volume for R50 specimens.

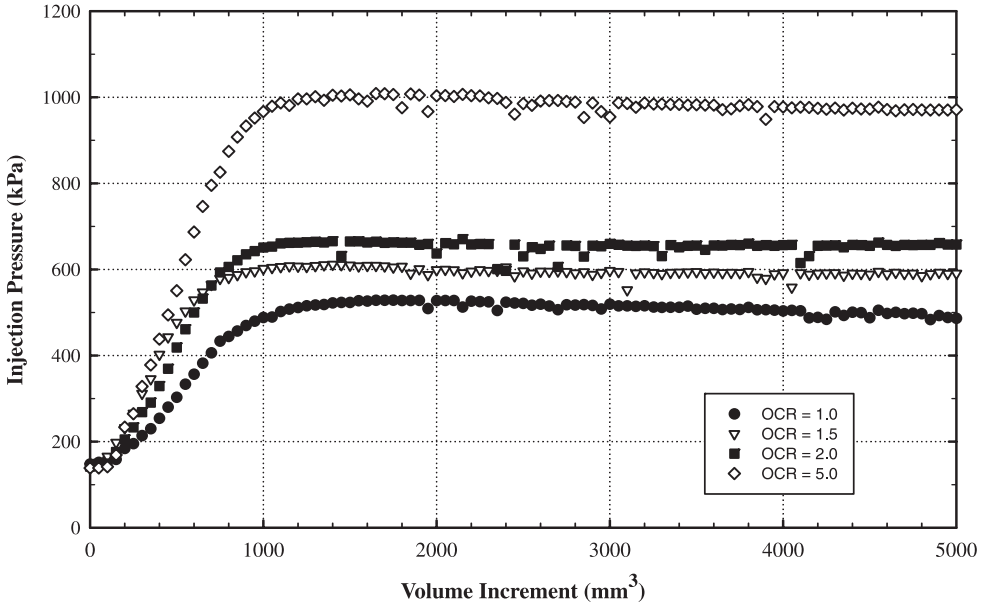

Fig. 10. Comparison of numerically simulated and experimentally measured peak injection pressure.

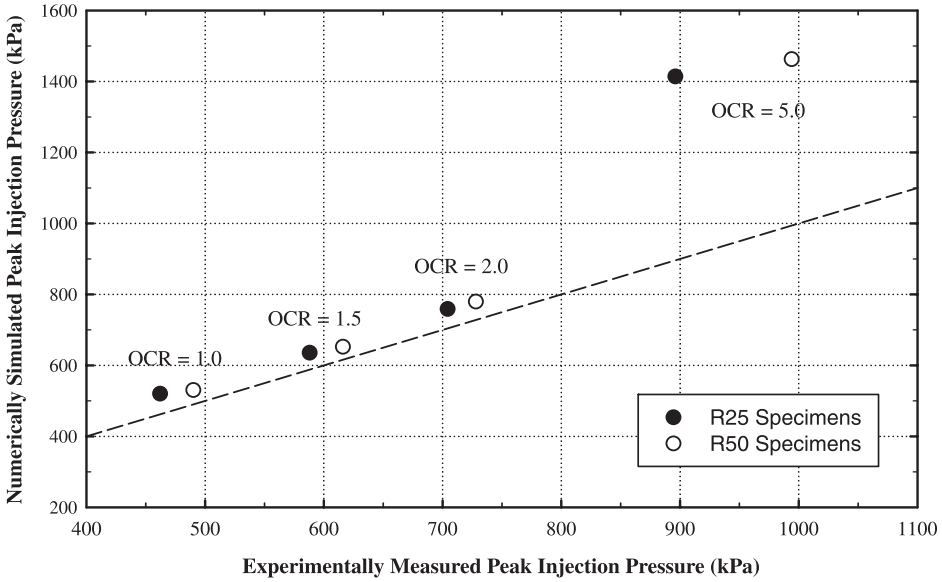

tance of 0.5 mm from the cavity boundary. Elements 2 and 3 are on the Z axis at a distance of 0.5 mm from the cavity boundary.

Variations of effective principal stresses in the numbered elements of a normally consolidated R50 specimen during the cavity expansion process are presented in Fig. 13. Results for the R25 specimen are very similar, indicating that the stress variation around the cavity is primarily controlled by the cavity itself. The indication is further substantiated by the observation that the results for elements 2 and 3 are practically identical, despite the different conditions of the top and bottom boundaries.

In element 1, the effective vertical stress (σ'_Z) and effective circumferential stress (σ'_T) decrease, and the effective horizontal stress, i.e., the effective radial stress (σ'_R), increases during the initial stage of cavity expansion, indicating that the increase in horizontal stress, i.e., radial stress, is considerably greater than those of vertical and circumferential stresses. Therefore, the expansion of the cavity is primarily in the horizontal direction. Moreover, the results also indicate that the increase in excess pore-water pressure is greater than the increase in total vertical stress and total circumferential stress, resulting in a decrease in effective vertical stress and effective circumferential stress. When the cavity volume is approximately 100 mm^3, the magnitudes of the principal stresses remain constant, indicating the clay has reached the critical state. Moreover, the changes in the magnitude of the three principal effective stresses during the cavity expansion process should be noted, as such changes cause rotation of maximum and minimum principal axes and an increase in deviatoric stress as a function of cavity volume.

The stresses in element 2 at the top of the cavity and ele-

Fig. 11. Average excess pore-water pressure around the cavity versus injection volume.

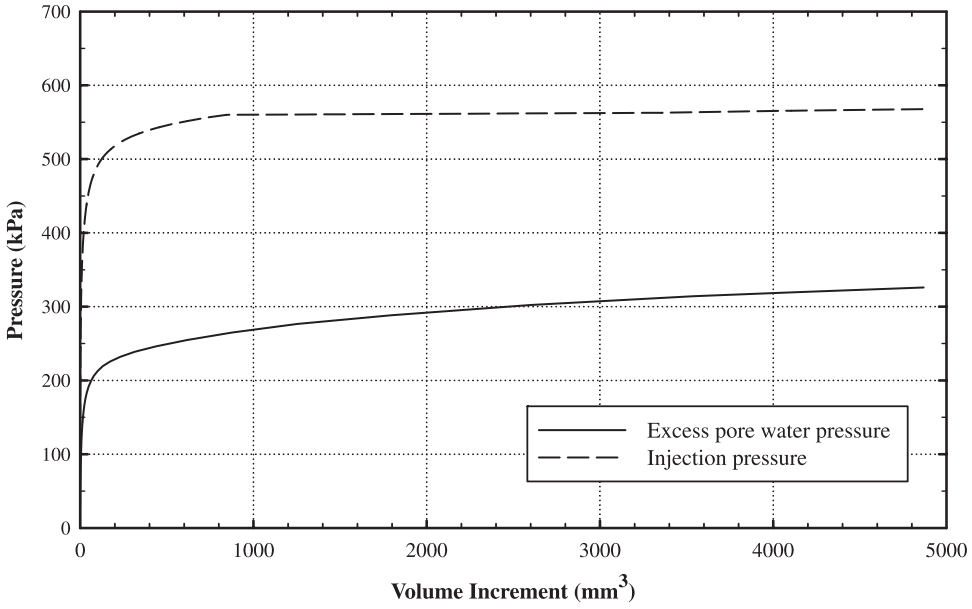

Fig. 12. Distribution of excess pore-water pressure along the R axis.

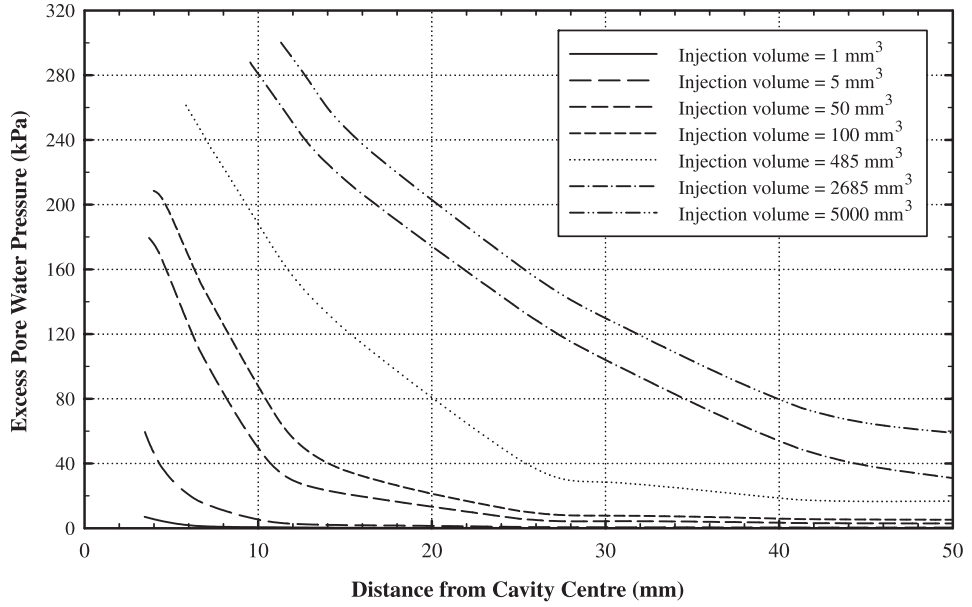

ment 3 at the bottom of the cavity are practically identical, indicating the effects of the different conditions of the top and bottom boundaries on the stress distribution in the immediate vicinity of the cavity are negligible. Moreover, the horizontal stress σ'_R and circumferential stress σ'_T are also practically identical due to symmetry. The effective vertical stress, i.e., effective radial stress, σ'_Z is always greater than the other two principal effective stresses in elements 2 and 3 as shown in Fig. 13, resulting in the expansion of the cavity in the vertical direction. However, $(\sigma'_Z - \sigma'_R)$ in elements 2 and 3 is greater than $(\sigma'_R - \sigma'_Z)$ in element 1. Therefore, the expansion in the vertical direction is greater than that in the horizontal direction, resulting in the formation of an elliptical cavity with a major axis in the vertical direction or CAR less than unity as depicted in Fig. 8. Moreover, the initial in situ horizontal stress is less than the vertical stress, as K_0 is less than unity, which is a favorable condition for the cavity to propagate in the vertical direction. Similar experimental results were reported by Alfaro and Wong (2001).

Variations of effective principal stresses of the numbered elements in a heavily overconsolidated R50 specimen during the cavity expansion process are presented in Fig. 14. In element 1, the effective horizontal stress, i.e., effective radial stress, σ'_R increases with an increase in cavity volume. The effective vertical stress σ'_Z and effective circumferential stress σ'_T decrease during the initial stage of cavity expansion, indicating that the increase in horizontal stress, i.e., radial stress, is considerably greater than the increases in vertical and circumferential stresses. Therefore, expansion of the cavity is in the horizontal direction. Moreover, the results

Fig. 13. Variation of effective principal stresses during cavity expansion for a normally consolidated R50 specimen.

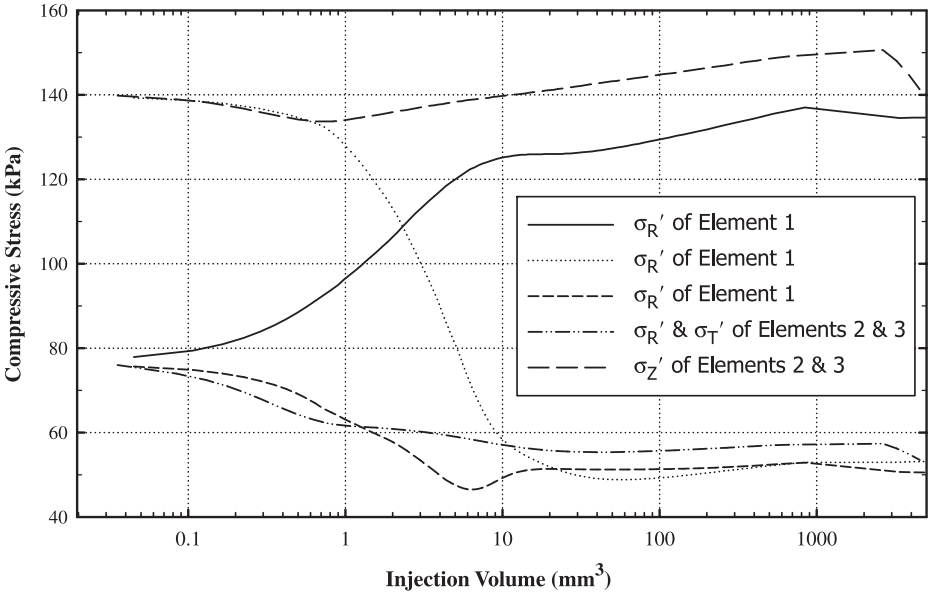

Fig. 14. Variation of effective principal stresses during cavity expansion for a heavily overconsolidated R50 specimen.

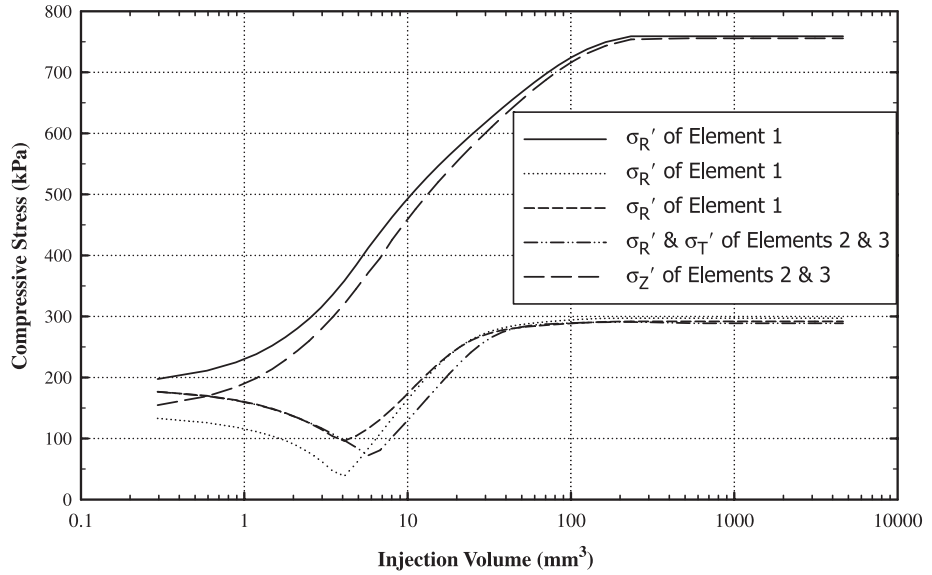

indicate that the increase in excess pore-water pressure is greater than the increases in total vertical stress and total circumferential stress during the initial stage of cavity expansion, resulting in decreases in the effective vertical stress and effective circumferential stress. Afterwards, both σ'_Z and σ'_T increase with an increase in cavity volume. When the cavity volume is approximately 300 mm^3, the magnitudes of the effective principal stresses remain constant, indicating the clay has reached the critical state.

The stresses in element 2 at the top of the cavity and element 3 at the bottom of the cavity are practically identical, indicating the effects of the different conditions of the top and bottom boundaries on the stress distribution in the immediate vicinity of the cavity are negligible. Moreover, the horizontal stress σ'_R and circumferential stress σ'_T are also practically identical due to symmetry. The effective vertical stress, i.e., effective radial stress, σ'_Z is always greater than the other two principal effective stresses in elements 2 and 3 as shown in Fig. 14, resulting in the expansion of the cavity in the vertical direction. However, $(\sigma'_Z - \sigma'_R)$ in elements 2 and 3 is slightly less than $(\sigma'_R - \sigma'_Z)$ in element 1. Therefore, the expansion in the horizontal direction is greater than that in the vertical direction, resulting in the formation of an elliptical cavity with a major axis in the horizontal direction or CAR slightly greater than unity, as depicted in Fig. 8. The initial in situ horizontal stress is greater than the vertical stress, however, as K_0 is greater than unity, resulting in the formation of a larger plastic zone in the vicinity of element 1 than that of elements 2 and 3. Therefore, CAR is only slightly greater than unity. In the R25 specimen, the effect of the boundary is more prominent, resulting in the formation of a larger plastic zone for the same injection volume in

Fig. 15. Schematic of simultaneous multiple-point injection.

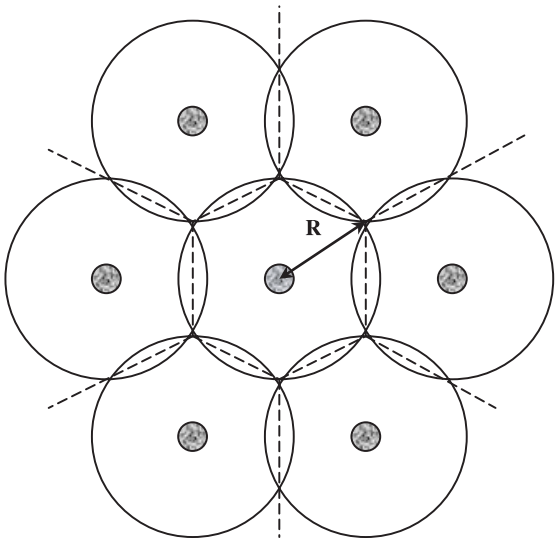

the vicinity of element 1. Therefore, CAR is much greater than unity, as shown in Fig. 8. Similar experimental results were reported by Alfaro and Wong (2001).

Potential practical applications of results

The results of this study can be used to develop a better understanding of the fundamental behaviour of compaction grouting in clay. It can be observed that the stress field, excess pore pressure distribution, and soil displacements during pressure-controlled cavity expansion vary as a function of injection volume. Moreover, these parameters may be affected by conditions of the outer boundary, resulting in different shapes of grout bulbs and different patterns of subsequent consolidation settlement. In real-life applications, there would not be a well-defined physical boundary to soil deformation as in the experimental study. The interactions between a single grout bulb and the rigid boundary, however, are analogous to those between a grout bulb and its neighboring grout bulbs in a closely spaced grid pattern as shown in Fig. 15. As the injection points are arranged in a closely spaced symmetrical array, overlapping of plastic zones or zones of excess pore pressure can be assumed to be symmetrical. Planes of symmetry shown as broken lines in Fig. 15 can be defined in each of these overlapping zones. These planes of symmetry can be considered as closed roller boundaries, as there is no drainage or soil displacement across the boundary. If the grouting points are arranged in a triangular array, the hexagonal boundary can be approximated as an equivalent circle. It is thus reasonable to simulate simultaneous multiple-point grout injection by a single injection within a circular boundary for much better computation efficiency. Therefore, the results obtained in this study can be applied to better understand the interactions between grout bulbs generated by a simultaneous multiple-point injection.

Conclusions

A numerical and experimental study on pressure-controlled cavity expansion in clay has been performed. The following conclusions are drawn from the study:

(1) The Cam-clay model is able to describe the behaviour of remolded clay with overconsolidation ratios (OCRs) ranging from 1 to 2 during pressure-controlled cavity expansion; however, the predictions made by the model deviate quite significantly from the experimental measurements for heavily overconsolidated clay.
(2) The cavity aspect ratio (CAR), defined as the ratio of the maximum horizontal dimension to the maximum vertical dimension of a grout bulb, is a reasonable parameter to characterize the shape of the grout bulb created by compaction grouting.
(3) The numerical simulation procedure developed in this study is a plausible tool in the prediction of clay behaviour during cavity expansion. Therefore, the approach can be utilized in other applications of pressure-controlled cavity expansion in geomechanics.
(4) The shape of the grout bulb created in clay by compaction grouting depends on the OCR of the clay, the state of stress of the ground, and the degree of lateral confinement.
(5) Both experimental results and numerical simulations indicate that the cavity propagates in the direction of maximum principal effective stress. It should be noted, however, that the direction of maximum principal effective stress may rotate during the cavity expansion process.

Acknowledgements

Financial support provided by Research Grants Council Project HKU 1178/03E of the Hong Kong Special Administrative Region Government for this project is gratefully acknowledged. However, the contents of this paper do not necessarily reflect the views and policies of the Research Grants Council of the Hong Kong Special Administrative Region Government, nor does the mention of trade names and commercial products constitute endorsement or recommendation for use.

References

Alfaro, M.C., and Wong, R.C.K. 2001. Laboratory studies on fracturing of low-permeability soils. Canadian Geotechnical Journal, **38**(2): 303–315.

Atkinson, J.H., and Bransby, P.L. 1978. The mechanics of soils. An introduction to critical state soil mechanics. McGraw-Hill, London, UK.

Au, S.K.A. 2001. Fundamental study of compensation grouting. Ph.D. dissertation, Department of Engineering, University of Cambridge, Cambridge, UK.

Au, S.K., Soga, K., and Yeung, A.T. 2006. A new laboratory apparatus for grout injection studies. Geotechnical Testing Journal, ASTM, **29**(2). In press.

Bolton, M.D., and Whittle, R.W. 1999. A non-linear elastic perfectly plastic analysis for plane strain undrained expansion tests. Géotechnique, **49**(1): 133–141.

Cao, L.F., The, C.I., and Chang, M.F. 2001. Undrained cavity expansion in modified Cam clay I: theoretical analysis. Géotechnique, **51**(4): 323–334.

Carter, J.P., Booker, J.R., and Yeung, S.K. 1986. Cavity expansion in cohesive frictional soils. Géotechnique, **36**(3): 349–353.

Chang, M.F., The, C.I., and Cao, L.F. 2001. Undrained cavity expansion in modified Cam clay II: application to the interpretation of the piezocone test. Géotechnique, **51**(4): 335–350.

Collins, I.F., and Stimpson, J.R. 1994. Similarity solutions for drained and undrained cavity expansion. Géotechnique, **44**(1): 21–34.

Collins, I.F., and Yu, H.S. 1996. Undrained cavity expansion in critical state soils. International Journal for Numerical and Analytical Methods in Geomechanics, **20**(7): 489–516.

El-Kelesh, A.M., Mossaad, M.E., and Basha, I.M. 2001. Model of compaction grouting. Journal of Geotechnical and Geoenvironmental Engineering, ASCE, **127**(11): 955–964.

Elmes, D.R. 1985. Creep and viscosity in two kaolin clays. Ph.D. thesis, Department of Engineering, University of Cambridge, Cambridge, UK.

Hill, R. 1950. The mathematical theory of plasticity. Clarendon Press, Oxford, UK.

Hsieh, Y.M., Whittle, A.J., and Yu, H.S. 2002. Interpretation of pressuremeter tests in sand using advanced soil model. Journal of Geotechnical and Geoenvironmental Engineering, ASCE, **128**(3): 274–278.

Kovacevic, N., Potts, D.M., and Vaughan, P.R. 2000. The effect of the development of undrained pore pressure on the efficiency of compaction grouting. Géotechnique, **50**(6): 683–688.

Salgado, R., and Randolph, M.F. 2001. Analysis of cavity expansion in sand. International Journal of Geomechanics, **1**(2): 175–192.

Schmidt, B. 1966. Discussion on "Earth pressures at rest related to stress history" by E.W. Brooker and H.O. Ireland. Canadian Geotechnical Journal, **3**(4): 239–242.

Schnaid, F., and Mantaras, F.M. 2003. Cavity expansion in cemented materials: structure degradation effects. Géotechnique, **53**(9): 797–807.

Soga, K., Au, S.K.A., Jafari, M.R., and Bolton, M.D. 2004. Laboratory investigation of multiple grout injections into clay. Géotechnique, **54**(2): 81–90.

Vesić, A.S. 1972. Expansion of cavities in infinite soil mass. Journal of the Soil Mechanics and Foundations Division, ASCE, **98**(3): 265–290.

Yu, H.S., and Houlsby, G.T. 1991. Finite cavity expansion in dilatant soils: loading analysis. Géotechnique, **41**(2): 173–183.

Yu, H.S., and Rowe, R.K. 1999. Plasticity solutions for soil behaviour around contracting cavities and tunnels. International Journal for Numerical and Analytical Methods in Geomechanics, **23**(12): 1245–1279.